Proceedings of the Combustion Institute, Volume 29, 2002/pp. 1419–1426

MEASUREMENT OF LAMINAR FLAME SPEEDS THROUGH DIGITAL PARTICLE IMAGE VELOCIMETRY: MIXTURES OF METHANE AND ETHANE WITH HYDROGEN, OXYGEN, NITROGEN, AND HELIUM

YUFEI DONG,[1] CHRISTINA M. VAGELOPOULOS,[2] GEOFFREY R. SPEDDING AND FOKION N. EGOLFOPOULOS[1]

[1]*Department of Aerospace and Mechanical Engineering*
University of Southern California
Los Angeles, CA 90089-1453, USA
[2]*Combustion Research Facility*
Sandia National Laboratories
Livermore, CA 94550, USA

A digital particle image velocimetry technique that is appropriate for the experimental derivation of fundamental flame properties was implemented. The technique allows for the determination of the instantaneous flowfield and is essential for fluid mechanics measurements in reduced gravity environments. Measurements of laminar flame speeds were conducted in the stagnation flow configuration just before a flame undergoes a transition from planar to Bunsen flame. Results obtained for lean CH_4/air and C_2H_6/air flames were found to be in close agreement with previous laser Doppler velocimetry data. Subsequently, measurements were conducted for the CH_4 and C_2H_6 flames by independently varying the equivalence ratio and flame temperature to distinguish between temperature and concentration effects. The laminar flame speeds were also calculated using the GRI-Mech 3.0 mechanism. It was convincingly shown that under high-O_2 and low-temperature conditions, the experimental laminar speeds are overpredicted by the simulations especially for C_2H_6 flames. Additional experiments were conducted by adding H_2 to lean C_2H_6/air flames and by diluting those mixtures by either He or N_2 to vary the flame temperature. While for the He dilution case, the predictions noticeably overpredict the experiments, for N_2 dilution, closer agreement was observed. Analyses of the flame structures revealed that for those fuel-lean flames, the burning rate largely depends on the competition of the two-body branching and three-body termination reaction between H and O_2. It was not possible to point to possible kinetic deficiencies other than referring to uncertainties associated with the rates and collision efficiencies of three-body reactions. The high-O_2 low-temperature region is of interest not only to lean-premixed combustion, but also to flame ignition, and requires further exploration.

Introduction

The accurate knowledge of the laminar flame speeds, S_u^o, of reacting mixtures is essential for validating chemical kinetics, for the modeling of turbulent combustion, and for the design of practical devices. S_u^o is defined as the propagation speed of a steady, laminar, adiabatic, one-dimensional, planar flame. The simplicity of this definition has caused controversy in the combustion community, as measured S_u^o values appeared to have a wide scatter [1]. It was subsequently realized [2,3] that while the effect of heat loss in most experiments was properly accounted for, the effect of flame stretch was not.

This led to the introduction of the counterflow technique for the S_u^o measurement [2,3] in which a reference flame speed, $S_{u,\mathrm{ref}}$, is first determined for a given value of the strain rate, K, defined as the maximum absolute value of the axial velocity gradient in the hydrodynamic zone. Varying $S_{u,\mathrm{ref}}$ with K for a given equivalence ration, ϕ, S_u^o is determined through extrapolations to $K = 0$. Improvements were subsequently implemented [4,5] to account for finite domain effects [6,7].

The need for extrapolations in the counterflow technique stems from the fact that steady flames cannot be stabilized at ultralow strain rates [8]. A *direct* measurement of S_u^o was achieved for the first time by Vagelopoulos and Egolfopoulos [8] (hereafter referred to as VE98) in the stagnation flow configuration, by imposing a transition from a positively stretched stagnation flame to a negatively stretched conical Bunsen flame. In doing so, the flame must pass through the zero stretch state. Subsequent direct numerical simulations by Cuenot, Egolfopoulos & Poinsot [9] (hereafter referred to as CEP01) confirmed that during this transition, the zero stretch rate state exists momentarily, with a propagation speed that coincides with S_u^o.

In the approaches of both extrapolation [2,3] and

transition [8], laser Doppler velocimetry (LDV) measurements were conducted along the stagnation streamline. LDV measurements can be rather accurate, but as point measurements, they cannot characterize the instantaneous flowfield. This is an important point, as when the transition method is used, the instantaneous strain rate cannot be quantified. Furthermore, the extrapolation technique becomes rather cumbersome and time-consuming. It should be also realized that under certain conditions, such as those encountered in reduced gravity facilities, there are significant time constraints that prohibit the use of LDV.

Digital particle image velocimetry (DPIV) techniques can, in principle, overcome such difficulties as the entire flowfield can be instantaneously quantified. Compared to LDV, DPIV requires equipment of higher level of sophistication including laser light source and pulsing, high-resolution cameras, the camera-laser synchronization electronics, and most important the image-processing software. The use of DPIV in laminar flames has been limited [e.g., Refs. 10–12], and archival data on fundamental flame properties have yet to appear. While the basic method is simple to implement, successful and reliable use requires a rigorous error analysis combined with algorithms that are suitably matched to measurement of high strain rates with potentially noisy and/or lossy data.

Again, in principle, successful implementation could revolutionize the way that fundamental flame properties are experimentally derived, as DPIV is more efficient than LDV and potentially more accurate and it provides better spatial and temporal resolution. More important, however, DPIV can result in the direct determination of flame properties, especially under transient conditions. Furthermore, the proper implementation of DPIV in microgravity facilities can also revolutionize microgravity combustion research as the fluid mechanics can be at last described locally. At present, global descriptions of the fluid mechanics are being used, such as, for example, global strain rates [e.g., Refs. 13,14].

Consequently, the primary goal of the present investigation was to introduce a DPIV technique whose properties are closely adapted for the accurate and efficient determination of fundamental flame properties. The details of the technique are presented next. The DPIV was first validated against previously derived laminar flame speeds using the LDV technique. Subsequently, laminar flame speeds of various fuel/air mixtures were determined as functions of the equivalence ratio and flame temperature. The experimental data were then compared with the results of detailed numerical simulations.

Experimental Approach

General Configuration and Procedures

The stagnation flow configuration was established between aerodynamically shaped nozzles and a stainless-steel stagnation plate. In a previous investigation [15], it was shown that as long as the flame is several flame thicknesses away from the plate, the effect of the downstream heat loss on S_u^o is negligible. Three nozzle diameters were used with $D =$ 14, 22, and 35 mm and $L/D = 1.5$, where L is the separation distance between the nozzle and the stagnation plane. The burner assembly was housed within an enclosure. For fuel-rich experiments, N_2 was used as ambient gas to prohibit the formation of non-premixed flames.

S_u^o's were determined by using the transition of a planar to a Bunsen flame as proposed by VE98. S_u^o is determined as the reference propagation speed, $S_{u,\mathrm{ref}}$, defined at the upstream boundary of the preheat zone of the flame just before the transition initiates to avoid complications introduced by flame curvature and motion. In addition to S_u^o, the DPIV provides the local strain rate, K, whose value is important in assessing the fidelity of the reported S_u^o. More specifically, for a given K the Karlovitz number $Ka \equiv D_m K/(S_u^o)^2$ can be estimated, where D_m is a characteristic mixture diffusivity. The lower the value of Ka, the closer is the measured flame speed $S_{u,\mathrm{ref}}$ to S_u^o. As shown in VE98 and CEP01, for values of Ka of the order of 10^{-3} or less $S_{u,\mathrm{ref}}$ is very close to the S_u^o value.

Correlation Imaging Velocimetry

Image acquisition

The data acquisition system was designed so that it contained only components that could readily be transferred to various low-g experimental facilities. Light from a continuous 5 W A+ laser was focused with a convex lens and spread into a slowly diverging light slice through two planoconcave elements. Particle seeding could not use gravity and so a mixing method using the existing gas intakes into the burner was devised. Al_2O_3 particles of 1–5 μm diameter were used. Numerical simulations were performed with a two-phase stagnation flow code [16], and results indicate that the particles closely follow the flow for the low range of the strain rates encountered in the experiments. A 768 $\times$ 484 CCD array camera (Pulnix-TN9701) with asynchronous reset and full-frame transfer allowed the DPIV timing to be regulated by timing pulses sent to a stand-alone, external optical shutter inserted into the light path before the first lens. A custom-built timing circuit synchronized alternate vertical drive pulses generated by the

camera to pulse pairs opening the polarization shutter at the end of one video frame and at the beginning of the next. The timing circuit determines the pulse interval, which was independently measured on an oscilloscope with less than 2% uncertainty. This pulse interval controls the particle image displacement magnitudes between successive frame pairs, which were analyzed using a custom DPIV method, described below. Within the constraints imposed principally by the available light, the system can be used for velocities up to 50 cm/s.

Correlation imaging velocimetry for estimating flow fields in cold jets and flames

Correlation imaging velocimetry (CIV) [17] describes a collection of techniques that is closely related to standard DPIV methods, but derived independently and with certain design differences that make it well suited to estimating complex, but almost two-dimensional, velocity fields (for which it was originally developed). Cross-correlations are computed between image pairs for arbitrary-sized rectangular boxes, whose size and shape are completely decoupled from the search domain of possible correlations. Correlation peaks are detected to subpixel accuracy by least-squares fitting spline-interpolated autocorrelation functions with the spline-interpolated cross-correlation. This results in significant reduction of the phase-locked peak-locking error (discussed in detail in Ref. [17]) that is the primary contributor to errors in measuring small displacements in all known DPIV methods. The raw velocity vectors are then numerically convected by their own flowfield over one-half the exposure interval and spline interpolated onto a regular, arbitrary grid by a thin-shell smoothing-spline technique [18]. Velocity components and their spatial derivatives are calculated at the grid points directly from the spline coefficients, without recourse to finite difference or post hoc filtering schemes.

Characteristics in flows with flames

Experiments are typically closely focused on the flame centerline, and a spatial resolution of 200 pixels/cm can be readily achieved. The correlation boxes are rectangular, with aspect ratio tuned to the predicted velocity gradients in the flow. Typical spatial resolutions are 0.5–1 mm for 20–30 measurements over a burner diameter and 30–45 along a centerline. Instantaneous velocity fields, and their gradients, are calculated directly from the spline coefficients. Since it is frequently a gradient quantity (strain rate) or a spatial location of an extremum that is required, it is particularly important to have a robust and accurate estimate of its value, and the spline interpolation allows this [17,18]. By contrast, the common alternative of calculating a noisy finite difference followed by smoothing is very likely to systematically underestimate velocity gradients. Similarly, systematic underestimation of extrema by averaging spatially non-stationary data can be avoided. Finally, since the peak location algorithm is a winner-take-all method on neighborhoods that converge around the likely correlation maximum, the estimate is unaffected by the self-correlation produced by the image of the flame front itself. An optical filter matched to the color of the flame is used on the camera lens to reduce flare and saturation of the pixels and maintain particle image contrast. The remaining flame front image has no effect on the displacement calculation. Beyond the flame front, temperature gradients produce refractive index variations that in turn modify the apparent particle image location, but the data are correct up to that point.

In summary, the CIV method has characteristics that match the operating requirements of the weakly burning, strained flame experiment in normal and in reduced gravity. The results that follow have been derived from these methods and have been cross-checked with LDV measurements where noted.

Numerical Approach

The PREMIX code [19] was used for the calculation of laminar flame speeds. The code has been modified to allow for thermal radiation from CH_4, CO, CO_2, and H_2O [20], and it is integrated with the CHEMKIN [21] and Transport [22] subroutine libraries. GRI-Mech 3.0 [23] was used to describe the kinetics.

As has also been previously reported [24], it was found that the accuracy of the calculated S_u^o depends on the spatial resolution of the simulations. The inset of Fig. 2 depicts that as the number of grid points increases, the calculated flame speed asymptotically reaches a limit that is defined as the numerically determined S_u^o. Overlooking this point can result in errors of 5–10%.

Results and Discussion

Experiments were conducted for atmospheric mixtures of CH_4 and C_2H_6 with H_2, O_2, N_2, and He. The experimental approach is shown in the four frames of Fig. 1. Fig. 1a depicts the flame topology, as it is about to undergo the transition to Bunsen flame. It can be seen that while the flame surface is planar around the centerline, it develops curvature at large radii in agreement with the simulations of CEP01. This curvature is a result of the shear layer that develops between the reacting jet with the ambient air [9]. Thus, three different spatial coordinates were utilized, namely, the axial, *x;* the radial, *r;* and the tangential to the flame surface, *s.*

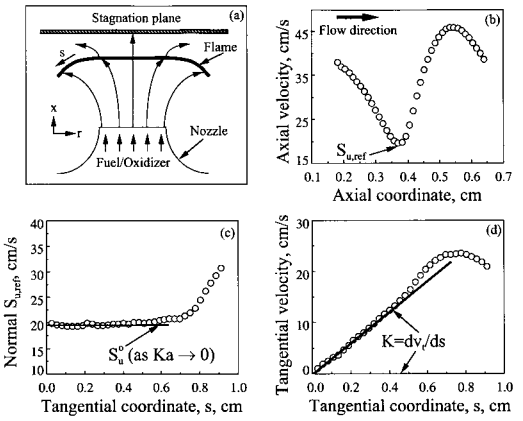

FIG. 1. Experimental schematic and procedure: (a) flame configuration and topology just before transition initiates; (b) typical axial velocity profile along the stagnation streamline; (c) variation of the normal to the flame surface reference flame speed, $S_{u,\mathrm{ref},n}$, with the tangential coordinate, s, and the determination of S_u^o; (d) variation of the tangential to the flame surface velocity, v_t, with the tangential coordinate, s, and the determination of the strain rate, K.

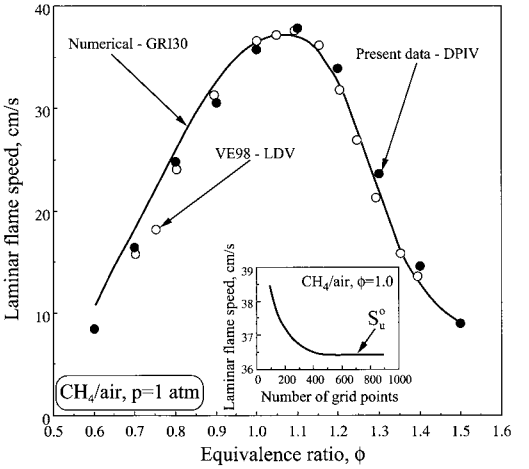

FIG. 2. Comparisons between the present experimental S_u^o data for atmospheric CH_4/air mixtures with those determined in VE98 and numerical predictions using GRI-Mech 3.0. (Inset) The dependence of the predicted S_u^o on the number of grid points used in the simulations.

Figure 1b depicts a typical axial velocity, u, profile along the stagnation streamline that intersects perpendicularly the (planar) flame surface. The minimum velocity is defined as a reference flame speed, $S_{u,\mathrm{ref}}$. CIV maps the instantaneous flame shape by identifying the relevant (x,r) pairs at the locations of $S_{u,\mathrm{ref}}$ before the flame. Subsequently, the total velocity vectors at those locations are projected normally and tangentially on to the flame surface, determining thus a normal reference flame speed, $S_{u,\mathrm{ref},n}$, and a tangential velocity, v_t, at this upstream boundary of the preheat zone.

The variations of $S_{u,\mathrm{ref},n}$ and v_t along the flame surface are shown respectively in Figs. 1c and 1d, in which the tangential coordinate s is used; note that s coincides with the radial coordinate r as long as the flame surface is planar. Fig. 1c depicts that $S_{u,\mathrm{ref},n}$ is nearly constant for a range of s and subsequently increases. The region of constant $S_{u,\mathrm{ref},n}$ corresponds to the planar segment of the flame surface and within this region the tangential velocity v_t varies linearly with s (i.e., r), as shown in Fig. 1d. The strain rate K is then determined as $K = dv_t/ds$ [12]. Note that the gradient of the tangential velocity component along the flame surface is by definition [e.g., Ref. 3] the flame stretch. The region within which $S_{u,\mathrm{ref},n}$ increases was found to correspond to the curved flame segment.

The laminar flame speed S_u^o is derived at the state just before the transition (to Bunsen flame) initiates, and this is the state of the lowest possible positive stretch. The values of $S_{u,\mathrm{ref},n}$ (Fig. 1c) are averaged up to the point where v_t no longer varies linearly with s (Fig. 1d), and the imposed (minimum) strain rate $K = dv_t/ds$ is evaluated. Using values of D_m that correspond to the thermal diffusivity of the mixture under standard conditions, the attending Ka numbers were derived. For all measurements reported, the Ka numbers were determined to be $1.0 \times 10^{-3} \leq Ka \leq 8.0 \times 10^{-3}$.

Figure 2 compares the present S_u^o's and those determined in VE98 with LDV for CH_4/air mixtures at various ϕ's. The two sets of data are in close agreement, which is an independent validation of the accuracy of the CIV-derived data. The numerically determined S_u^o's are also shown in Fig. 2, and close agreement can be seen in general. Note, however, that there is a systematic overprediction of the experimental S_u^o's as the mixture becomes progressively leaner.

The discrepancies between experimental and predicted S_u^o for very lean mixtures have not attracted proper attention, as the observed differences of 1–2 cm/s are typically considered to lie within experimental uncertainties. This is because as ϕ decreases, S_u^o decreases as a result of the flame temperature reduction. Thus, if S_u^o is to be used for validating chemical kinetics for a wide range of ϕ's, the proper way to do it is by keeping the flame temperature constant as ϕ changes so that concentration effects are isolated from that of temperature [25].

Figure 3 depicts experimental and predicted S_u^o's for $CH_4/O_2/N_2$ mixtures as functions of ϕ, keeping the adiabatic flame temperature, T_{ad}, constant by modifying the relative O_2/N_2 free-stream concentrations; T_{ad} was determined by equilibrium calculations. For all three T_{ad} investigated, 1900, 2000, and

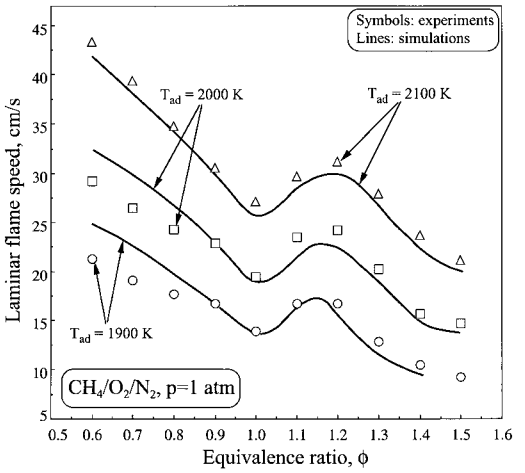

FIG. 3. Variation of experimental and predicted S_u^o with equivalence ratio, ϕ, for atmospheric $CH_4/O_2/N_2$ mixtures under conditions of constant adiabatic flame temperature achieved by modifying the relative O_2:N_2 concentrations in the oxidizer.

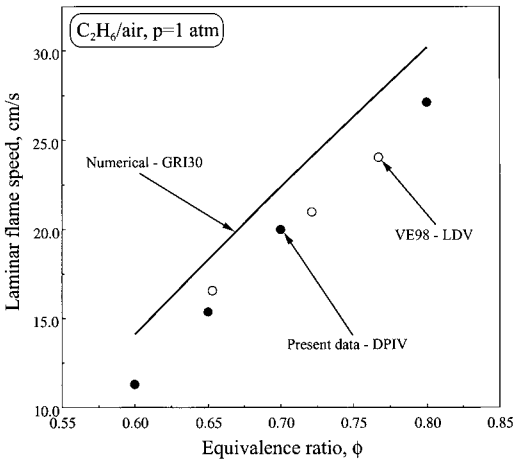

FIG. 4. Comparisons between the present experimental S_u^o data for fuel-lean atmospheric C_2H_6/air mixtures with those determined in VE98 and numerical predictions using GRI-Mech 3.0.

2100 K, S_u^o exhibits a non-monotonic behavior. For $\phi < 1$ mixtures, S_u^o increases as ϕ decreases. Species consumption and sensitivity analyses showed that as ϕ decreases the rate of the main branching reaction

$$H + O_2 \rightarrow OH + O \qquad (R1)$$

is enhanced as the O_2 concentration increases for the same T_{ad}. For $\phi > 1$ mixtures, S_u^o first increases and then decreases as ϕ increases. S_u^o increases because the O_2 concentration increases relatively to N_2 to maintain the same T_{ad}. Thus, the rate of reaction R1 is enhanced. Subsequently, the mixture reactivity is reduced as the CH_4 concentration increases to the point that it effectively scavenges H radicals through reaction

$$CH_4 + H \rightarrow CH_3 + H_2 \qquad (R1)$$

competing, thus, for H radicals with reaction R1 whose rate is reduced. As a result, the burning rate is also reduced.

Comparing the experimental and predicted S_u^o's, it can be seen that there is a close agreement for near-stoichiometric and rich flames. It is interesting, however, that while for lean flames the agreement is very close for $T_{ad} = 2100$ K, for the lower T_{ad}'s, the experiments are noticeably overpredicted by the simulations. The observed discrepancies are greater than the experimental uncertainty, which is less than 3% (as measured by the maximum difference between the maximum and minimum S_u^o values derived from repeated experiments).

As expected, analyses of lean flames with $\phi = 0.6$ revealed that for all T_{ad}'s, S_u^o is particularly sensitive to the competition between the main branching reaction R1 (highest positive sensitivity on S_u^o) and the three-body termination reaction:

$$H + O_2 + M \rightarrow HO_2 + M \qquad (R3)$$

with M = H_2O having the greatest negative sensitivity on S_u^o. It was also found that this sensitivity increases as T_{ad} decreases, but it was not possible to identify a distinctly different kinetics behavior between the 1900 and 2100 K that could point to a possible deficiency. It should be noted, however, that the third-body efficiencies associated with reaction R3 are not well characterized, and this could be a possible source of the observed discrepancies.

S_u^o's of lean C_2H_6/air mixtures were also measured, and the results are shown in Fig. 4 along with the measurements of VE98 and numerical predictions. The close agreement between the two sets of experimental S_u^o values is apparent. It can be also seen that the numerical simulations overpredict the experimental values more noticeably compared to the lean CH_4/air flames shown in Fig. 2.

The effect of T_{ad} on S_u^o was also addressed by keeping ϕ fixed and varying the relative concentration of O_2:N_2 in the oxidizer. The results are shown in Fig. 5 for both $CH_4/O_2/N_2$ and $C_2H_6/O_2/N_2$ mixtures with $\phi = 0.6$ and $\phi = 1.0$. It can be seen that while experiments and simulations are in very close agreement for $\phi = 1.0$, the experimental values are systematically overpredicted by the simulations for $\phi = 0.6$ and for lower T_{ad}'s. Fig. 5 also depicts the effect of He dilution on S_u^o at various T_{ad}'s for stoichiometric CH_4/air and C_2H_6/air flames; the use of He was motivated by the results of Fig. 7 that will be shown below. It can be seen that the experimental S_u^o values are noticeably overpredicted for both

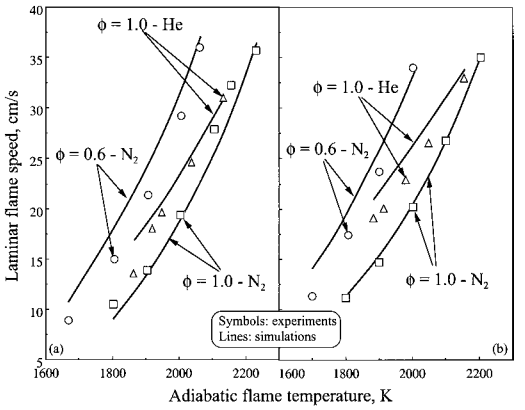

FIG. 5. Variation of experimental and predicted S_u^o's with adiabatic flame temperature for atmospheric: (a) $\phi = 0.6$ and $\phi = 1.0$ $CH_4/O_2/N_2$ mixtures (ϕ = 0.6-N_2, ϕ = 1.0-N_2) and $\phi = 1.0$ CH_4/air/He mixtures (ϕ = 1.0-He); (b) $\phi = 0.6$ and $\phi = 1.0$ C_2H_6/air/He mixtures (ϕ = 0.6-N_2, ϕ = 1.0-N_2) and $\phi = 1.0$ C_2H_6/air/He mixtures (ϕ = 1.0-He). The adiabatic flame temperature was varied by adjusting the relative O_2:N_2 concentrations in the oxidizer for the ϕ = 0.6-N_2 and ϕ = 1.0-N_2 cases and by diluting with He the C_2H_6/air mixture for the ϕ = 1.0-He case.

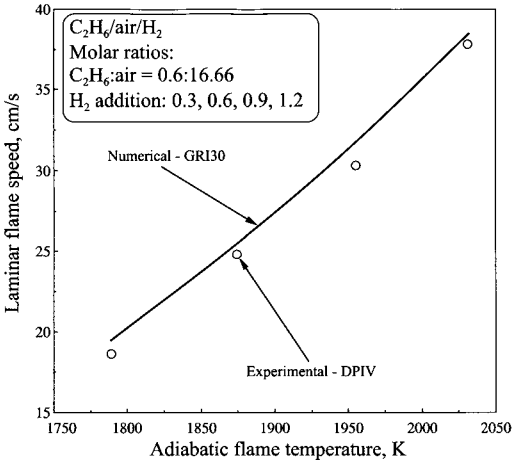

FIG. 6. Variation of experimental and predicted S_u^o's with adiabatic flame temperature for atmospheric $C_2H_6/air/H_2$ mixtures, through H_2 addition in a $\phi = 0.6$ C_2H_6/air flame. Molar ratios, C_2H_6:air 0.6:16.66. The four experimental points correspond to H_2 molar addition of 0.3, 0.6, 0.9, and 1.2.

CH_4/air/He and C_2H_6/air/He flames as He dilution increases and T_{ad} decreases.

Sensitivity analyses of lean C_2H_6 flames revealed that similarly to CH_4 flames, S_u^o is mostly sensitive to reactions R1 and R3. However, it was found that the reaction

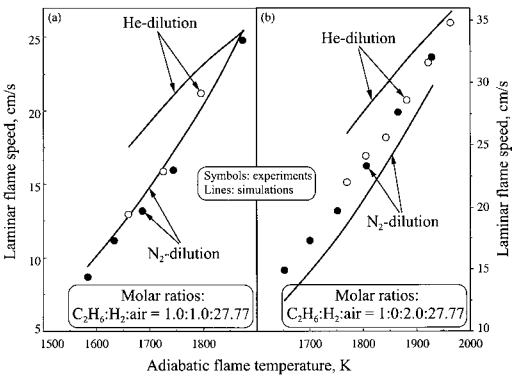

FIG. 7. Variation of experimental and predicted S_u^o's with adiabatic flame temperature for atmospheric N_2-diluted and He-diluted C_2H_6/H_2/air mixtures and for the following molar ratios: (a) C_2H_6:H_2:air 1.0:1.0:27.77; (b) C_2H_6:H_2:air 1.0:2.0:27.77.

$$C_2H_5 + H \rightarrow CH_3 + CH_3 \qquad (R4)$$

also has a significant negative sensitivity on S_u^o for C_2H_6 flames; C_2H_6 consumption results readily in C_2H_5 whose main consumption path is reaction R4.

The systematic overprediction of S_u^o by GRI-Mech 3.0 for fuel-lean conditions, especially for C_2H_6 flames, was further assessed. A $\phi = 0.6$ C_2H_6/air mixture was considered, in which various amounts of H_2 were added resulting in higher S_u^o's, which were subsequently reduced by diluting the C_2H_6/H_2/air mixture either by N_2 or by He, similarly to the results of Fig. 5. H_2 was added to further enhance the importance of H_2/O_2 chemistry that largely affects S_u^o, even for hydrocarbon flames. Helium was used as diluent along with N_2 as its use can moderate *Le* number effects that the H_2 addition can have on the flame dynamics.

Figure 6 depicts experimental and predicted S_u^o's for four different H_2 molar additions without inert dilution, and a close agreement can be seen. The effect of inert dilution is shown in Fig. 7 that depicts experimental and predicted S_u^o's for two different H_2 molar additions, C_2H_6:H_2 1:1 (Fig. 7a) and 1:2 (Fig. 7b). The results show that for both cases, the experimental S_u^o's are significantly overpredicted for He dilution, especially at lower T_{ad}'s, similarly to the results of Fig. 5. For N_2 dilution, however, it can be seen that the experimental S_u^o's are closely predicted for the lower H_2 addition (Fig. 7a) and moderately underpredicted for the higher H_2 addition (Fig. 7b). Analyses of the flame structures resulting from He and N_2 dilution did not reveal any particular differences between the sensitivities and contributions to the species consumption of the controlling reactions. Note that in all simulations, the contribution from the Soret effect was included. Furthermore, in the He dilution simulations, the third-body efficiency of

He was taken to be equal to that of Ar of GRI-Mech 3.0. It is also of interest that the experimental S_u^o's for both He and N_2 dilution lie on a single curve, indicating the dominant effect of T_{ad}, which, however, is not reproduced by the simulations. For the levels of He addition that were used in the experiments of Fig. 7, the molecular transport effect on S_u^o through the $(\lambda/c_p)^{1/2}$ term was found to be minor (<6%), comparing states with He and N_2 dilution levels that result in the same T_{ad}, where λ and c_p are the mixture's conductivity and specific heat, respectively.

Concluding Remarks

An accurate and efficient DPIV technique was introduced for the measurement of fundamental flame properties. Its use is essential for characterizing the instantaneous flowfield but also for experimental conditions such as the ones encountered in reduced gravity environments in which the experimental times are short to accommodate point measurements. A CW A+ laser, an optical chopper, and an asynchronous CCD array camera were used. Particle image displacements were computed using the CIV algorithms, where accurate estimation of gradient quantities is also emphasized.

The system was tested in normal gravity by measuring laminar flame speeds in the stagnation flow configuration by determining the propagation speed and the attendant strain rate just before the transition of a planar flame to a Bunsen flame initiated. Results showed very close agreement with previous results for CH_4/air and C_2H_6/air flames obtained through LDV.

Laminar flame speeds were also determined by independently varying the equivalence ratio and flame temperature, to decouple thermal and concentration effects. For low flame temperatures, GRI-Mech 3.0 noticeably overpredicts the laminar flame speeds of lean CH_4/O_2/inert and C_2H_6/O_2/inert mixtures. Additional experiments were conducted with lean C_2H_6 flames, in which various amounts of H_2 were added. Subsequently, those flames were diluted with He and N_2, and the laminar flame speeds were measured at various flame temperatures. It was found that for He dilution, the GRI-Mech 3.0 significantly overpredicts the experimental data. For N_2 dilution, closer agreement was found.

The observed discrepancies in the fuel-lean regime that is also characterized by low flame temperatures were assessed through sensitivity and species consumption analyses. It was found that the competition of the main branching and three-body termination reactions between H and O_2 largely controls propagation, as expected. However, based on GRI-Mech 3.0, it was not possible to identify a distinctly different response of the kinetics to the various conditions tested.

This issue requires further investigation, as the high-O_2 low-temperature regions are not only relevant to lean-premixed combustion, but also to flame ignition. Possible causes may be traced to the formulation of the rates of three-body termination reactions and in particular into the current understanding of the magnitude and possible temperature dependence of third-body collision efficiencies.

Acknowledgments

This work was supported by NASA (grant NAG3-1615) under the technical supervision of Dr. Fletcher Miller of the Glenn Research Center and by AFOSR (grant F49620-02-1-0002) under the technical supervision of Dr. Julian M. Tishkoff.

REFERENCES

1. Andrews, G. E., and Bradley, D., *Combust. Flame* 18:133–153 (1972).
2. Wu, C. K., and Law, C. K., *Proc. Combust. Inst.* 20:1941–1949 (1984).
3. Law, C. K., *Proc. Combust. Inst.* 22:1381–1402 (1988).
4. Vagelopoulos, C. M., Egolfopoulos, F. N., and Law, C. K., *Proc. Combust. Inst.* 25:1341–1347 (1994).
5. Chao, B. H., Egolfopoulos, F. N., and Law, C. K., *Combust. Flame* 109:620–638 (1997).
6. Dixon-Lewis, G., *Proc. Combust. Inst.* 23:305–324 (1990).
7. Tien, J. H., and Matalon, M., *Combust. Flame* 84:238–248 (1991).
8. Vagelopoulos, C. M., and Egolfopoulos, F. N., *Proc. Combust. Inst.* 27:513–519 (1998).
9. Cuenot, B., Egolfopoulos, F. N., and Poinsot, T., "Direct Numerical Simulation of Stagnation-Flow Premixed Flames: Transition from Planar to Bunsen Flames," paper 134, U.S. Sections Second Joint Meeting of the Combustion Institute, Oakland, CA, March 25–28, 2001.
10. Reuss, D. L., Adrian, R. J., and Landreth, C. C., *Combust. Sci. Technol.* 67:73–83 (1989).
11. Mueller, C. J., Driscoll, J. F., Reuss, D. L., Drake, M. C., and Rosalik, M. E., *Combust. Flame* 112:342–358 (1998).
12. Hirasawa, T., Sung, C. J., Wang, H., and Law, C. K., "Determination of Laminar Flame Speeds Using Digital Particle Image Velocimetry," paper 284, U.S. Sections Second Joint Meeting of the Combustion Institute, Oakland, CA, March 25–28, 2001.
13. Maruta, K., Yoshida, M., Ju, Y., and Niioka, T., *Proc. Combust. Inst.* 26:1283–1289 (1996).
14. Zhang, H., and Egolfopoulos, F. N., *Proc. Combust. Inst.* 28:1875–1882 (2000).
15. Egolfopoulos, F. N., Zhang, H., and Zhang, Z., *Combust. Flame* 109:237–252 (1997).

16. Egolfopoulos, F. N., and Campbell, C. S., *Combust. Flame* 117:206–226 (1999).
17. Fincham, A. M., and Spedding, G. R., *Exp. Fluids* 23:449–462 (1997).
18. Spedding, G. R., and Rignot, E. J. M., *Exp. Fluids* 15:417–430 (1993).
19. Kee, R. J., Grcar, J. F., Smooke, M. D., and Miller, J. A., Sandia report SAND85-8240.
20. Law, C. K., and Egolfopoulos, F. N., *Proc. Combust. Inst.* 24:137–144 (1992).
21. Kee, R. J., Rupley, F. M., and Miller J. A., Sandia report SAND89-8009.
22. Kee, R. J., Warnatz, J., and Miller, J. A., Sandia report SAND83-8209.
23. Bowman, C. T., Frenklach, M., Gardiner, W. R., and Smith, G., *The GRI 3.0 Chemical Kinetic Mechanism,* 1999, www.me.berkeley.edu/gri mech/.
24. Egolfopoulos, F. N., and Law, C. K., *Proc. Combust. Inst.* 23:333–340 (1990).
25. Zhu, D. L., Egolfopoulos, F. N., and Law, C. K., *Proc. Combust. Inst.* 22:1537–1545 (1988).